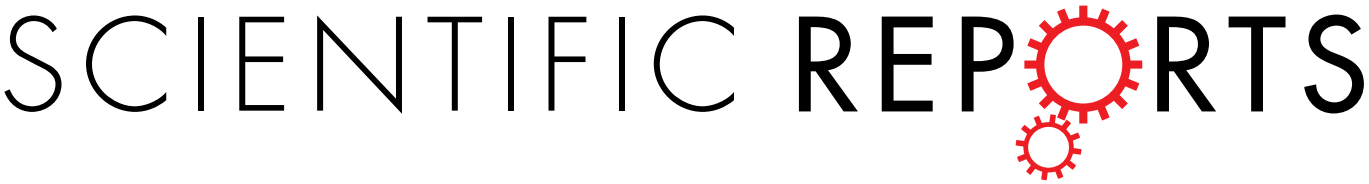

OPEN

Efficient Synthesis of Ethanol from CH_4 and Syngas on a Cu-Co/TiO_2 Catalyst Using a Stepwise Reactor

Received: 18 April 2016
Accepted: 16 September 2016
Published: 03 October 2016

Zhi-Jun Zuo[1], Fen Peng[1,2] & Wei Huang[1]

Ethanol synthesis from CH_4 and syngas on a Cu-Co/TiO_2 catalyst is studied using experiments, density functional theory (DFT) and microkinetic modelling. The experimental results indicate that the active sites of ethanol synthesis from CH_4 and syngas are Cu and CoO, over which the ethanol selectivity is approximately 98.30% in a continuous stepwise reactor. DFT and microkinetic modelling results show that $*CH_3$ is the most abundant species and can be formed from $*CH_4$ dehydrogenation or through the process of *CO hydrogenation. Next, the insertion of *CO into $*CH_3$ forms $*CH_3CO$. Finally, ethanol is formed through $*CH_3CO$ and $*CH_3COH$ hydrogenation. According to our results, small particles of metallic Cu and CoO as well as a strongly synergistic effect between metallic Cu and CoO are beneficial for ethanol synthesis from CH_4 and syngas on a Cu-Co/TiO_2 catalyst.

Owing to the diminishing supply of fossil fuels and rising crude oil prices, an alternative fuel source must be developed. Ethanol synthesis has recently attracted increasing attention because of its nontoxic nature and ability to be produced from renewable sources[1]. In general, there are two main methods of ethanol synthesis: one is fermentation derived from corn or sugar cane and hydration of petroleum-based ethylene, and the other is CO hydrogenation[1–6]. Ethanol synthesis from syngas has recently received attention owing to food shortages. To the best of our knowledge, Rh-based catalysts are the best catalysts that show relatively high ethanol selectivity[7–10]. However, the high cost of Rh limits its application in industry.

C_2-oxygenate synthesis from CH_4 and CO_2 is thermodynamically unfavourable at low temperatures, but this can be overcome through a stepwise reaction technology that has been proposed by our group[11]. In this process, $*CH_4$ is first adsorbed on the catalyst surface (M) and then dissociated to generate CH_x-M; subsequently, the $*CO_2$ species is inserted into the C-M bond to form $*CH_xCOO$ before finally forming acetic acid from $*CH_xCOO$ hydrogenation[12–14]. It was found that the Pd-Co and Cu-Co bi-metal supported on TiO_2 catalysts exhibited good activity for acetic acid from CH_4 and CO_2[15]. Because CO_2 has a relatively high reduction potential (1.9 V to CO_2^-), the conversion is difficult[16]. If CO_2 is replaced by CO, then the conversion of CO is possibly better than that of CO_2. Therefore, we propose a method of ethanol synthesis from CH_4 and syngas in a stepwise reactor.

Although the activity of the Pd-Co/TiO_2 catalysts is better than that of the Cu-Co/TiO_2 catalysts for acetic acid synthesis from CH_4-CO_2 in the stepwise reactor[15], we chose the Cu-Co/TiO_2 catalysts for ethanol synthesis from CH_4 and syngas, considering the price of Pd. Finally, the reaction mechanisms of ethanol from CH_4 and syngas were studied on Cu-Co/TiO_2 using density functional theory (DFT) and microkinetic modelling. The result may be useful for computational design and optimizations of Cu-Co/TiO_2 catalysts.

Result and Discussion

Experimental result. Figure 1 shows the H_2-TPR profile of the Cu-Co/TiO_2 catalyst before reaction. The H_2-TPR curves show four main peaks. The peak at 178 °C can be assigned as the reduction of CuO to Cu, and the peak at 238 °C is attributed to Cu–Co spinal phase (such as $Cu_xCo_{3-x}O_4$ oxides)[4,17]. The peaks at approximately 276 and 394 °C are assigned the reduction of $Co_3O_4 \rightarrow CoO$ and $CoO \rightarrow Co$[18–20]. Note that the reduction temperatures of $Co_3O_4 \rightarrow CoO$ and $CoO \rightarrow Co$ are approximately 450 and 550 °C[18], which are higher than that of our catalyst. The reason for this observation is that the Cu species are first reduced at low temperatures to form metallic Cu nanoparticles, which subsequently catalyse the reduction of nearby Co species[18,19]. As a result, the reduction temperature of the Co species in the Cu-Co/TiO_2 catalyst is lower than that of the pure Co species. No reduction

[1]Key Laboratory of Coal Science and Technology of Ministry of Education and Shanxi Province, Taiyuan University of Technology, Taiyuan 030024, Shanxi, China. [2]Key Laboratory of Renewable Energy and Gas Hydrate, Guangzhou Institute of Energy Conversion, Chinese Academy of Sciences, Guangzhou, China. Correspondence and requests for materials should be addressed to W.H. (email: huangwei@tyut.edu.cn)

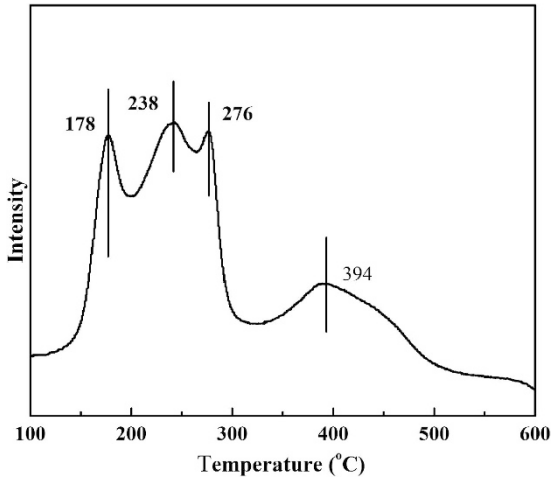

Figure 1. H_2-TPR profile before reaction.

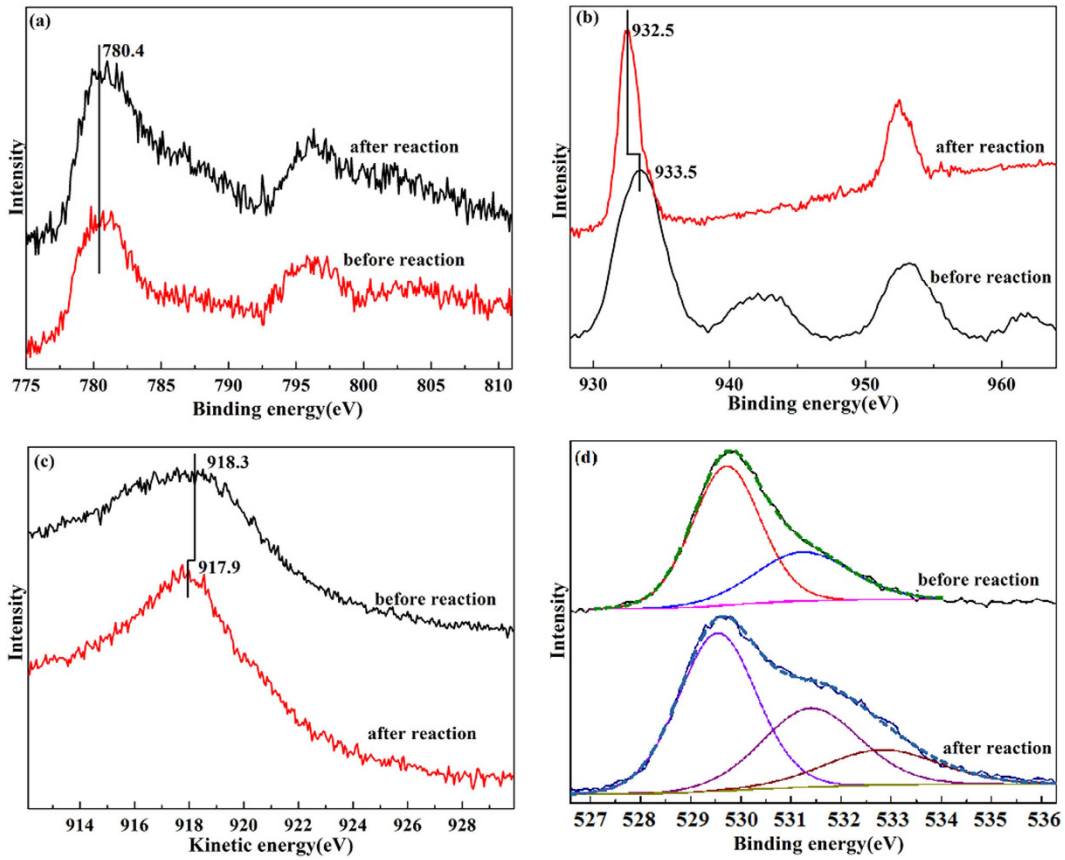

Figure 2. Co 2p (**a**), Cu 2p (**b**), Cu LMM (**c**) and O 1s (**d**) XPS spectra before and after reaction.

peak of TiO_2 is detected, which is in accordance with our X-ray powder diffraction (XRD) (Fig. S1) results. XRD and high-resolution transmission electron microscopy (TEM) (Fig. S2) also show that Cu species and Co species are uniformly dispersed on the catalyst surface.

Figure 2 displays the Co 2p, Cu 2p, Cu LMM, and O 1s XPS spectra of the Co-Cu/TiO_2 catalyst before and after reaction. As shown in Fig. 2a, the binding energies of Co 2p3 before and after are similar to each other, being located at approximately 780.4 eV. The intensity of the shakeup satellite of Co 2p3 before the reaction is obviously lower than that after the reaction. Therefore, the Co species before the reaction is mainly Co_3O_4 and Cu–Co spinal phase, a similar shape of the Co 2p3/2 core level spectra is also observed for mixed $Cu_xCo_{3-x}O_4$ oxides[21–23]. After reaction, CoO is the main phase[21,24]. This result is similar to our previous result, in which CoO is the main phase in the Co-Pd/TiO_2 catalysts under 400 °C for a 2 h reduction using *in-situ* XPS[21]. Note that some CoO is reduced

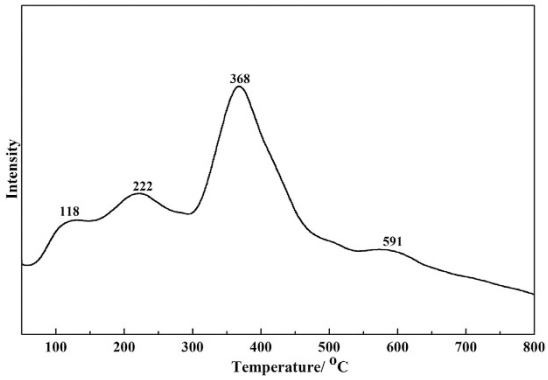

Figure 3. NH_3-TPD before reaction.

	CH_3OH	C_2H_5OH	CH_3COOH	C_2H_6	H_2O
STY	1.90	139.37	0.51	—[c]	—
selectivity[a]	1.34	98.30	0.36	—	—
s[b]	11.23	88.77	0	0	0

Table 1. The STY ($mg \cdot g_{cat.}^{-1} \cdot h^{-1}$) and selectivity (%) of products on Cu-Co/TiO_2 catalyst. [a]Experiment result. [b]Microkinetic modeling. [c]Not detected by experiment.

to metallic Co at 400 °C according to the TPR result, but the metallic Co is not detected by XPS. The reason for this observation is that a small amount of CoO is reduced at approximately 400 °C, i.e., much CoO is not reduced, according to the TPR result. Thus, the Co 2p3 peak of CoO overlaps with that of metallic Co, and the intensity of CoO is larger than that of metallic Co; as a result, the metallic Co is not detected by XPS.

For Cu 2p (Fig. 2b), a shakeup satellite is observed at approximately 942 eV before the reaction, and the binding energy of Cu 2p3 before the reaction is approximately 933.5 eV, which can be assigned to Cu^{2+} (CuO, 933.7 eV)[25,26]. The result shows that the surface is covered by CuO before the reaction. After the reaction, the shakeup satellite disappears, indicating that the CuO is reduced. The metallic Cu and Cu_2O cannot be distinguished using Cu 2p3, whereas they could be distinguished from the Cu LMM Auger spectra (Fig. 2c). As shown in Fig. 2c, the kinetic energy of Cu LMM after the reaction is approximately 917.9 eV. The kinetic energy is slightly smaller than the kinetic energy of metallic Cu (918.4 eV) but is obviously larger than that of Cu_2O (916.2 eV)[25,26]. This result indicates that the surface is covered by metallic Cu after the reaction. The kinetic energy of Cu LMM is approximately 918.3 eV, which is similar to the kinetic energy of CuO (918.1 eV)[25,26], further verifying the presence of CuO on the surface before the reaction.

In the case of O 1s (Fig. 2d), the peaks at 529.7 and 531.3 eV are assigned as lattice oxygen and O(H) species respectively before reaction[27]. After reaction, a new peak appears at 532.7 eV. The peak can be attributed to C=O or O-C-O[28], because the productions adsorb on the surface. For the Ti species, the binding energies are approximately 458.5 eV before and after the reaction (Fig. S3), which can be assigned to the TiO_2[29]. The result shows that the TiO_2 could not be reduced during the reaction. In general, the surface is mainly covered by CuO and Co_3O_4 before the reaction, whereas the surface is mainly covered by Cu and CoO after the reaction, in agreement with the H_2-TPR result. In other words, the metallic Cu and CoO are the active sites for the CH_4-syngas conversion.

Figure 3 shows the NH_3-TPD spectra of the Cu/TiO_2 catalyst. A larger peak and four main NH_3 desorption peaks are detected. The first peak at approximately 118 °C is attributed to the weak acid, the second and third peaks are assigned to the mediate strong acid, and the peak at 591 °C is assigned to the strong acid. Our group has been studying the activation and conversion of CO_2 and CH_4 over Cu-Co catalysts supported on different solid acid supports, such as γ-Al_2O_3, ZrO_2/SO_4^{2-}, and HZSM5[30]. The activation ability of CH_4 on the Cu-Co catalyst increases with increasing acid intensity, but the too strong acid is not beneficial for the formation of active species. In other words, the appropriate acid intensity of the Co-Cu/TiO_2 catalyst is favours for the conversion of CH_4 and syngas.

Table 1 shows the formation rate and the selectivity of the products on the Cu-Co/TiO_2 catalyst. As shown in Table 1, the formation rates of CH_3OH, C_2H_5OH and CH_3COOH are 1.90, 139.37 and 0.51 $mg \cdot g_{cat.}^{-1} \cdot h^{-1}$, respectively, and the corresponding selectivities of CH_3OH, C_2H_5OH and CH_3COOH are 1.34%, 98.30% and 0.36%, respectively. The result shows that the formation rate and selectivity of C_2H_5OH are far greater than those of CH_3OH and CH_3COOH, indicating that the Cu-Co/TiO_2 catalyst is beneficial for the formation of C_2H_5OH. In addition, only C_2H_5OH, CH_3OH, and CH_3COOH are produced; these species are easily separated.

DFT results. *Ethanol synthesis from CH_4 and syngas on CoCu(111) surface.* The adsorption configurations of possible intermediates involved ethanol synthesis from CH_4 and syngas on the CoCu(111) surface are shown in Fig. S4, and the corresponding adsorption parameters are listed in Table 2. Figures S5–S10 show the energy barriers, the reaction energies and the TS structures of ethanol synthesis from CH_4 and syngas on the CoCu(111) surface.

Species	E_{ads}	$d_{Cu\text{-}X}$ (Å)[a]	$d_{Co\text{-}X}$(Å)	Adsorption site
CH_4	−0.11			—
CH_3	−1.69		2.214	bri_{Co}
CH_2	−4.23	2.153	2.058	fcc_{Co}
CH	−5.81	2.065	1.958	fcc_{Co}
C	−6.43		1.924	bri_{Co}
H	−2.67	1.874	1.764	fcc_{Co}
CO	−1.27		2.030	bri_{Co}
CO_2	−0.53		−1.924	top_{Co}
H_2O	−0.08			—
CHO	−1.76		2.203	bri_{Co}
COH	−2.72	2.153	1.971	fcc_{Co}
O	−3.94	2.012		fcc_{Cu}
CH_2O	−0.26			—
CHOH	−2.21		2.083	bri_{Co}
CH_3O	−1.92		2.125	bri_{Co}
CH_2OH	−1.43		2.118	top_{Co}
CH_3OH	−0.51		2.467	top_{Co}
C_2H_6	−0.24			—
CH_3CO	−1.88		2.052	top_{Co}
	−1.82	2.039		top_{Cu}
CH_2CO	−1.67	2.256	2.124	fcc_{Co}/C(-H)-bri_{Co},C(-O)-top_{Cu}
CHCO	−3.12	2.384	2.037	fcc_{Co}/C(-H)-bri_{Co},C(-O)-top_{Cu}
CCO	−4.94	2.147	1.979	fcc_{Co}
CH_3COH	−2.34		1.987	top_{Co}
CH_3CHO	−0.59		2.040	top_{Co}
CH_3CHOH	−1.75		2.171	top_{Co}
C_2H_5OH	−0.43		2.289	top_{Co}
CH_3COO	−0.92		2.073	bri_{Co}/O-top_{Co}, O-top_{Co}
CH_3COOH	−0.27			—

Table 2. The adsorption energies (E_{ads}, eV) and adsorption configurations (d, Å) of possible intermediates at their preferable adsorption sites. [a]The nearest bond length, X stands for H, C or O.

As shown in Figs S5 and S6, $*CH_4$ dehydrogenation are as follows: $*CH_4 \rightarrow *CH_3 \rightarrow *CH_2 \rightarrow *CH \rightarrow *C$, which is in accordance with the previous studies of CH_4 dehydrogenation on different metals and alloys using DFT[31–39]. Table S1 shows the adsorption parameters of $*CH_4$, $*CH_3$, $*CH_2$, *CH and *C on a Cu site. Comparing Table 2 with Table S1, the binding strengths of $*CH_3$, $*CH_2$, *CH and *C on a Co site (−1.69, −4.23, −5.81 and −6.43 eV) are found to be obviously larger than those on a Cu site (−1.23, −3.82, −5.21 and −5.46 eV); the binding strength of *H on a Co site (−2.67 eV) is slightly larger than that on a Cu site (−2.45 eV); and the binding strength of $*CH_4$ on a Co site (−0.11 eV) is similar to that on a Cu site (−0.10 eV). The observed trend is in agreement with the result of Liu *et al.*[37]. We also studied $*CH_3$ and $*CH_2$ formation on fcc_{Cu} (Fig. S7); the energy barriers are 1.92 and 1.18 eV, which are far larger than that on a Co site. The result indicates that CH_4 dehydrogenation prefers to occur on Co sites versus Cu sites.

As shown in Fig. S8, *CHO and $*CH_2O$ formation are likely from *CO hydrogenation. Again, $*CH_2O$ hydrogenation is superior to dissociation. Because the energy barrier of $*CH_3O$ formation (0.89 eV) is similar to that of $*CH_2OH$ formation (0.82 eV), $*CH_2OH$ and $*CH_3O$ further reactions are considered. In the case of $*CH_2OH$ further reaction, $*CH_2$ formation occurs slightly easier than $*CH_3OH$ formation. Similarly, $*CH_3O$ prefers to be dissociated into $*CH_3$ and *O. A previous study showed that the energy barrier of $*CH_3O + *H \rightarrow *CH_3OH + *$ (0.76 eV) is lower than that of $*CH_3O + * \rightarrow *CH_3 + *O$ (1.05 eV) on a Rh(111) surface[40]. The energy barrier of $*CH_3O + *H \rightarrow *CH_3OH + *$ (1.07 eV) is obviously smaller than that of $*CH_3O + * \rightarrow *CH_3 + *O$ (2.22 eV) on a Cu(211) surface; however, the energy barrier of $*CH_3O + *H \rightarrow *CH_3OH + *$ (1.41 eV) is slightly lower than that of $*CH_3O + * \rightarrow *CH_3 + *O$ (1.67 eV) on a Rh doped Cu(211) surface. Thus, Zhang *et al.* considered that C-O scission is difficult to perform on Cu-based catalysts and the promoter Rh facilitates $*CH_3$ formation. The results show that the promoter Rh increases the productivity and selectivity of ethanol synthesis from syngas on Cu-based catalysts[41]. The energy barrier and reaction energy of $*CH_3OH + * \rightarrow *CH_3 + *OH$ are 0.81 and 0.10 eV, and the energy barrier of $*CH_3OH + * \rightarrow *CH_3 + *OH$ is higher than that of the desorption energy of CH_3OH (0.51 eV). This result shows that CH_3OH desorption occurs on the surface.

According to the above results, $*CH_3$, $*CH_2$, *CH and *C are the possible intermediates during the process of $*CH_4$ dehydrogenation, and $*CH_3$ and $*CH_2$ are the possible intermediates from C-O scission during the process of methanol from syngas. Therefore, $*CH_3$, $*CH_2$, *CH and *C reactions with *CO are considered in this section. As shown in Fig. S9, the energy barriers of $*CH_3CO$, $*CH_2CO$, *CHCO and *CCO are in the following order: $*CH_3CO$ (0.49 eV) > $*CH_2CO$ (1.55 eV) > *CHCO (1.71 eV) > *CCO (2.07 eV). The result shows that the

No.	Elementary reactions	E_a	No.	Elementary reactions	E_a
1	$CH_4(g) + * \rightarrow CH_4*$		12	$CH_2* + H* \rightarrow CH_3* + *$	0.61
2	$CO(g) + * \rightarrow CO*$		13	$CH_4* + * \rightarrow CH_3* + H*$	1.28
3	$H_2(g) + 2* \rightarrow 2H*$		14	$CH_3* + CO* \rightarrow CH_3CO* + H*$	0.49
4	$CO* + H* \rightarrow CHO* + *$	1.09	15	$CH_3CO* + H* \rightarrow CH_3COH* + *$	0.86
5	$CHO* + H* \rightarrow CH_2O* + *$	0.72	16	$CH_3COH* + H* \rightarrow CH_3CHOH* + *$	0.62
6	$CH_2O* + H* \rightarrow CH_3O* + *$	0.89	17	$CH_3CHOH* + H* \rightarrow C_2H_5OH(g) + *$	0.28
7	$CH_2O* + H* \rightarrow CH_2OH* + *$	0.82	18	$CO* + O* \rightarrow CO_2* + *$	0.81
8	$CH_3O* + * \rightarrow CH_3* + O*$	0.62	19	$CH_3* + CO_2* \rightarrow CH_3COO* + *$	1.13
9	$CH_3O* + H* \rightarrow CH_3OH(g) + 2*$	1.17	20	$CH_3COO* + H* \rightarrow CH_3COOH* + *$	0.93
10	$CH_2OH* + * \rightarrow CH_2* + OH*$	1.09	21	$H* + OH* \rightarrow H_2O(g) + *$	1.43
11	$CH_2OH* + H* \rightarrow CH_3OH(g) + 2*$	1.38	22	$CH_3* + CH_3* \rightarrow C_2H_6(g) + *$	0.89

Table 3. The optimal reaction pathways for ethanol synthesis on CoCu(111) surface together with the corresponding activation barriers(E_a, eV).

insertion ability of *CO decreases with decreasing H number of $*CH_x$(x = 0, 1, 2, 3). Finally, $*C_2H_5OH$ is synthesized through $*CH_3COH$ and $*CH_3CHOH$ from $*CH_3CO$ further hydrogenation (Fig. S10).

It is well known that the Cu-based catalysts also have applications in the water-gas shift (WGS) reaction or the reverse WGS reaction[42–44]. Because of the complication of both reactions, we only consider $*CO_2$ and $*H_2O$ formation. The energy barriers of $*CO + *O \rightarrow *CO_2 + *$ and $*OH + *H \rightarrow *H_2O + *$ are 0.81 and 1.43 eV, respectively (Fig. S10). The energy barrier of $*CH_3 + *CO_2 \rightarrow *CH_3COO + *$ are 1.13 eV, which is higher than those of $*CH_3CO$ (0.49 eV) and $*C_2H_6$ (0.89 eV) formation, indicating that CH_3COO formation is difficult. There is only one product of $*CH_3COO$ hydrogenation, $*CH_3COOH$, for which the energy barrier and reaction energy are 0.93 and 0.08 eV, respectively.

Ethanol synthesis from CH_4 and syngas on Cu(111) and Co(111) surfaces. According to the above result, there are two key factors for ethanol synthesis: one is $*CH_x$ formation; the other is C-C bond formation. For $*CH_x$ formation, there are two methods: one is from CH_4 decomposition; the other is from C-O bond scission during the process of methanol synthesis. Liu *et al.* studied CH_4 decomposition on Co(111) and Cu(111) surfaces[37]. They found that the energy barrier of $*CH_3$ formation from $*CH_4$ dehydrogenation on a Cu(111) surface is obviously higher than that on a Co(111) surface (1.14 vs. 1.88 eV) using the same calculation parameters. The results show that CH_4 decomposition preferably occurs on a Co site.

Regarding $*CH_x$ formation during the process of methanol synthesis from syngas, our previous results showed that the energy barriers of $*CH_3OH$ and $*CH_3$ formation from $*CH_3O$, $*CH_3O$ and $*CH_2$ formation from $*CH_2O$, and $*CH_2O$ and *CH formation from *CHO on a Cu(111) surface are 0.63 and 2.18 eV, 1.00 and 2.05 eV, and 0.93 and 2.05 eV, respectively[45]. Zhang *et al.* and Mehmood *et al.* studied ethanol synthesis from a Cu(211) surface and methanol decomposition on Cu_4 nanoparticles; they also found that the ability of hydrogenation is greater than that of C-O scission[41,46]. The result indicates that $*CH_x$ is not formed on a Cu(hkl) surface during methanol synthesis. In the case of a Co surface, Mehmood *et al.* proposed that the energy barriers of $*CH_3OH$ and $*CH_3$ formation from $*CH_3O$, $*CH_3O$ and $*CH_2$ formation from $*CH_2O$, and $*CH_2O$ and *CH formation from *CHO on Co_4 nanoparticle are 1.48 and 1.66 eV, 0.86 and 1.11 eV, and 1.43 and 2.13 eV, respectively[46]. The energy barriers of $*CH_3OH$ and $*CH_3$ formation from $*CH_3O$ and $*CH_3O$ and $*CH_2$ formation from $*CH_2O$ are similar to each other, but the energy barrier of *CH formation is higher than that of $*CH_2O$ formation. The result shows that $*CH_2$ and $*CH_3$ species formation are likely on a Co surface.

According to the above results, it was found that the formation of *CH, $*CH_2$ and $*CH_3$ during the process of $*CH_4$ dehydrogenation and $*CH_3OH$ formation on a single Co active site are possible; however, it is impossible on a single Cu active site. Therefore, we only consider C-C formation on the Co(111) surface. The energy barriers, reaction energies and TSs are shown in Fig. S11.

Fig. S11 shows that the energy barriers of $*C_2H_6$, $*CH_3CO$, $*CH_2CO$ and *CHCO formation are 0.76, 1.04, 1.40 and 2.02 eV, respectively. Comparing the energy barriers of C-C formation on the CoCu(111) surface, it was found that the energy barriers of $*C_2H_6$ (0.76 vs. 0.89 eV) and $*CH_2CO$ (1.40 vs. 1.55 eV) formation on the Co(111) surface are slightly lower than those on the CoCu(111) surface, whereas the energy barriers of $*CH_3CO$ (1.04 vs. 0.49 eV) and *CHCO (2.02 vs. 1.71 eV) formation on the Co(111) surface are higher than those on the CoCu(111) surface. The result also shows that Co-Cu based catalysts change the reaction path. In addition, the energy barrier of $*C_2H_6$ formation is lower than those of $*CH_3CO$, $*CH_2CO$ and *CHCO formation. The result shows that $*C_2H_6$ formation is preferable, for which hydrocarbon formation is preferred versus C_2 oxygenate. The result is in agreement with the experiment results in which a Co-based catalyst is one of catalysts for the F-T reaction[47–49]. Therefore, ethanol synthesis from CH_4 and syngas requires two active sites: CoO and metallic Cu. In addition, because ethanol synthesis from CH_4 and syngas requires a synergistic effect between metallic Cu and CoO, small particles of CoO and metallic Cu are required.

Microkinetic modelling. To date, most possible reactions during the reaction of CH_4 and syngas have been studied using DFT. Table 3 summarises the optimal reaction pathways for ethanol synthesis on the CoCu(111) surface together with the corresponding activation barriers. In this section, to estimate the results from DFT, the selectivity of the possible products involved in ethanol synthesis from CH_4 and syngas under our experimental

condition was studied using a microkinetic model[50]. Similar kinetic modelling has been successfully applied for various reactions[40,51,52]. As shown in Table 3, the adsorption processes (R1, R2 and R3) are assumed to be in equilibrium. The other surface species involved in the R4-R22 reaction can be described according to the pseudo-steady-state approximation[50]. The relative selectivity (s) values are defined as $s_i = r_i/_i$, where r is the relative rate for each product, and i denotes CH_3OH, C_2H_5OH, C_2H_6, CH_3COOH and H_2O. The detailed description of the microkinetic model is shown in the supplement.

According to our DFT results and the microkinetic model, the relative selectivity of CH_3OH, C_2H_5OH, C_2H_6, CH_3COOH and H_2O are determined under our experimental conditions ($P_{CH4} = 0.95$ atm, $P_{CO} = 0.5$ atm, $= 0.5$ atm and $T = 300$ °C). As shown in Table 1, the relative selectivities of CH_3OH and C_2H_5OH are 11.23 and 88.77%; the relative selectivities of C_2H_6, CH_3COOH and H_2O are very small and can be ignored. Compared with the experiment result, it is found that the selectivity of CH_3OH using the microkinetic model is higher than that the experiment result, whereas the selectivities of C_2H_5OH and CH_3COOH using the microkinetic model are lower than the experiment results. The differences in selectivity between our theoretical and experimental results could be caused by many effects. The first possible reason is that the Cu-Co alloy is not formed during 400 °C calcinations[53,54], and the experiment results show that the Cu-CoO interface is the best model. The second possible explanation for the selectivity differences between our theoretical and experimental results is the presence of defect sites. To our best knowledge, defects can have a major role in catalysis by affecting the energy barriers[55–58]. Nonetheless, ethanol synthesis from CH_4 and syngas on CoCu(111) provides useful insights into the experiment to a certain degree. In the future, we plan to investigate the Cu-CoO interface and defects for ethanol synthesis from CH_4 and syngas.

Conclusions

In the paper, ethanol synthesis from CH_4 and syngas on a CoCu-based catalyst was studied using experiments, DFT and microkinetic modelling. The experimental results indicated that ethanol can be synthesised at high efficiency from CH_4 and syngas on the Cu-Co/TiO_2 catalyst, over which the selectivity of ethanol is approximately 98.30%. It was found that the active sites of ethanol synthesis are metallic Cu and CoO, with metallic Cu and CoO uniformly dispersed on the catalyst surface.

Most possible ethanol formation pathways from methanol and syngas were systematically investigated on CoCu(111) surface. The DFT result showed that ethanol synthesis from CH_4 and syngas requires the synergistic effect between metallic Cu and CoO, and ethanol is not synthesised on single metallic Cu and CoO. On the CoCu(111) surface, $*CH_3$ is the primary CH_x species. $*CH_3$ forms via three pathways: the first is $*CH_4$ dehydrogenation, the second is C-O scission of $*CH_3O$, and the third is CH_2 hydrogenation from C-O scission of $*CH_2OH$. Subsequently, $*CH_3CO$ forms from the *CO and $*CH_3$ reaction. Finally, ethanol is synthesised through $*CH_3COH$ hydrogenation. The microkinetic modelling result showed that there is only CH_3OH and C_2H_5OH, for which the selectivity of ethanol is lower than that of the experiment result. We think that the difference between the theoretical and experimental results could be mainly caused by issues with the model and the presence of defect sites. Future work will focus on the Cu-CoO interface and defects for ethanol synthesis from CH_4 and syngas.

Experimental and theoretical methods. *Catalyst preparation.* The preparation of the support TiO_2 was as follows: 24 g of NaOH was introduced into 60 mL of distilled water (10 M NaOH solution), and then, 1.0 g of commercial TiO_2 powder (P25, Degussa) was dispersed into the 10 M NaOH solution with continuous stirring for 2 h. The mixture was transferred into a Teflon-lined autoclave, and then, the mixture was heated to 150 °C for 24 h under sealed conditions. Subsequently, the mixture was allowed to cool to room temperature. The powder was washed using distilled water until the pH of the powder was approximately 7. The neutral powder was washed using 0.1 mol/L HNO_3 and then washed again using distilled water until the pH of the powder was approximately 7. After drying for 10 h at 75 °C, the obtained precipitate was calcined in air at 400 °C for 10 h, and the heating rate was 1 °C /min. Finally, the support TiO_2 was obtained[59,60].

The preparation method of the Cu-Co/TiO_2 catalyst was the equal volume impregnation method. TiO_2, $Co(NO_3)_2{\cdot}6H_2O$ and $Cu(NO_3)_2{\cdot}3H_2O$ were dissolved into ethylene glycol solution. After stirring for 12 h, the resulting slurry was dried for 12 h at 150 °C. Subsequently, the catalyst was calcined in air at 400 °C for 4 h at the heating rate of 2 °C/min. Finally, the Cu-Co/TiO_2 catalyst was obtained[21]. The Cu and Co loading on TiO_2 were 12 and 6 wt.%.

Catalyst characterization. XPS was performed using a V.G. Scientific ESCALAB250 with focused monochromated Al Kα. The residual pressure inside the analysis chamber was set to $< 2.0 \times 10^{-9}$ mbar. For H_2 temperature-programmed reduction (TPR) experiment, 50 mg catalyst was loaded into a fixed-bed reactor. The heating rate was 10 °C/min until the temperature is 600 °C using a temperature controller. The reduction gas was H_2 and N_2 which the ratio was 5:95 with a flow rate of 30 mL/min. NH_3-TPD experiment was used on a TP-5000 instrument. 100 mg catalyst adsorbed NH_3 at 50 °C until saturation, then purged the physisorbed NH_3 using He for 30 min. Finally, the NH_3-TPD data were collected in flow He from 50 to 800 °C which the heating rate was 10 °C/min.

Catalytic activity test. The diagram of the reaction apparatus is shown in Fig. 4 and was the same as the reaction apparatus of our previous paper on acetic acid synthesis from CH_4 and CO_2[12]. There was 1.5 g of catalysts used in reactor A and B, respectively. Before the reaction, the catalyst in both reactor A and B was reduced with 30 vol % H_2 and 70 vol % N_2 at 400 °C for 2 h. Because H_2 was found to inhibit the excessive dehydrogenation of methane during CH_4 activation, CH_4 and H_2 were injected together[12]. The reaction was carried out at 300 °C at atmospheric pressure. The test procedure is as follows: first, 50 ml/min of CH_4 and 5 ml/min of H_2 were injected into reaction

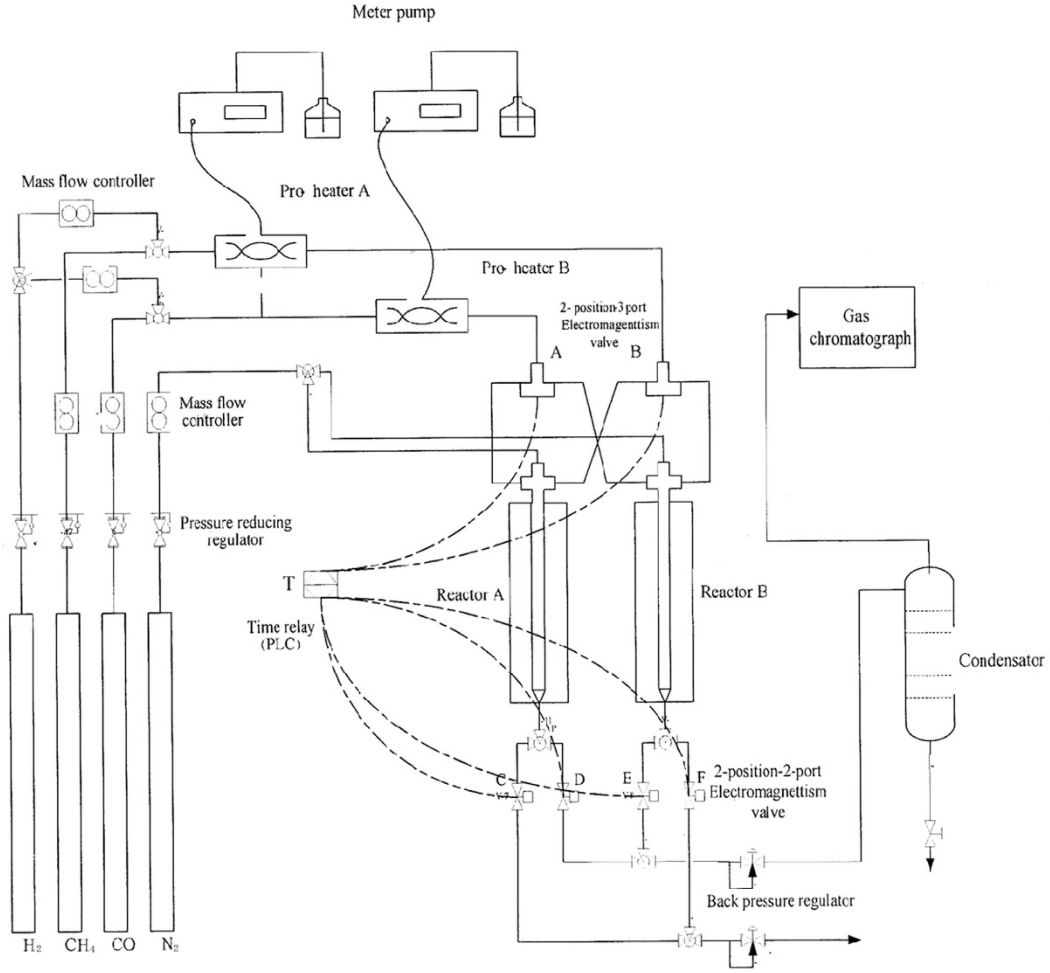

Figure 4. Schematic diagram of the experimental apparatus.

A; at the same time, syngas (50 ml/min of CO and 50 ml/min of H_2) were injected into reaction B. After 300 s, the electromagnetic valve was changed over. Then, syngas (50 ml/min of CO and 50 ml/min of H_2) were injected into reaction A, and at the same, 50 ml/min of CH_4 and 5 ml/min of H_2 were injected into reaction B. Subsequently, the cycle was repeated until the reaction was finished, and ethanol was produced from CH_4 and syngas.

The obtained products from the reaction were analysed using a gas chromatograph (GC-950) equipped with a hydrogen flame detector and packed column. The contents of each component were studied using the external standard method. On-line gas phase analysis and off-line analysis of the liquid products were performed, with the off-line analysis assisting in the product identification. The detailed analysis procedure used is as follows. The products were cooled by a condensator. Next, the liquid products were obtained from the condensator every hour and were injected into the GC. The gas phase was collected every 70 s; the gas was not cooled and condensed by the condensator. Only the oxy-organics in the gas phase were considered. The space time yield (STY, S), the number of total moles of the hydrocarbon (n), and the selectivity of carbon atoms (x) were defined as $S = K \times A \times V/m$, $n =$ and $x = S \times N/(n \times M)$, where K, A, V, m, N and M are a constant using the external standard method, the area of products (i) using chromatography, gas flow, mass of catalyst, carbon number of the products and molar mass of products, respectively.

Computational methods. The geometries and transition state (TS) were calculated using the Dmol^3 Materials Studio software[61,62]. The calculation parameters were the same as those in our previous studies[45,63]. The electronic structures were obtained by solving the Kohn−Sham equation self-consistently under spin-unrestricted conditions[64,65]. DFT was also used for the core electrons by applying the PW91 generalised-gradient approximation to the exchange-correlation energy[66]. A double numeric quality basis set with polarisation functions was used. A self-consistent field procedure is carried out with a convergence criterion of 10^{-5} a.u. on energy and electron density, and the geometry is optimized under a symmetry constraint, with the convergence criteria of 10^{-3} a.u. on the gradient and 10^{-3} a.u. on the displacement. The TS was identified using the complete linear/quadratic synchronous transit method[67].

The Cu(111) surface was cleaved from the face-centred cubic (fcc) crystal structure after optimisation; the theoretical equilibrium lattice constant of Cu was $a_{Cu} = 3.685$ Å, compared with the experimental value of

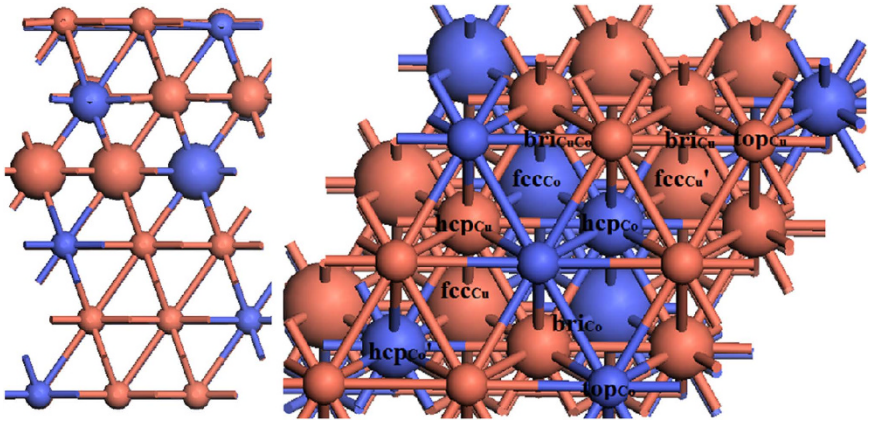

Figure 5. Side view (left) and top (right) view of the CoCu(111) surface after optimization.

$a_{Cu} = 3.604$ Å[68]. The surface was modelled using a six-layered mode p(3 × 3) super cell with nine atoms in each layer along with a 15 Å vacuum slab. The mass ratio of Cu:Co was 2 in the experiment, for which the molar ratio was approximately 1.8, and the molar ratio of Cu:Co of the CoCu(111) surface was 2 to simplify the model building. Next, three Cu atoms were replaced by Co atoms in each of the layers. The structure of the CoCu(111) surface after optimisation is shown in Fig. 5. During the calculation process, the bottom two layers were fixed, and other layers and adsorbates were allowed to relax. Meshes of 3 × 3 × 1 k-points were used for the CoCu(111) and Co(111) surfaces.

References

1. Hansen J. Ø. *et al.* Unravelling site-specific photo-reactions of ethanol on rutile TiO_2(110), *Sci. Rep.* **6,** 21990 (2016).
2. Sun, J., Wan, S., Wang, F., Lin, J. & Wang, Y. Selective synthesis of methanol and higher alcohols over Cs/Cu/ZnO/Al_2O_3catalysts. *Ind. Eng. Chem. Res.* **54,** 7841–7851 (2015).
3. Zuo, Z. J., Wang, L., Yu, L. M., Han, P. D. & Huang, W. Experimental and theoretical studies of ethanol synthesis from syngas over CuZnAl catalysts without other promoters. *J. Phys. Chem. C* **118,** 12890–12898 (2014).
4. Zuo, Z. J., Wang, L., Liu, Y. J. & Huang, W. The effect of CuO–ZnO–Al_2O_3 catalyst structure onthe ethanol synthesis from syngas. *Catal. Commun.* **34,** 69–72 (2013).
5. Gao, W. *et al.* Catalytic conversion of syngas to mixed alcohols over CuFe-based catalysts derived from layered double hydroxides. *Catal. Sci. Technol.* **3,** 1324–1332 (2013).
6. Wang, J., Chernavskii, P. A., Khodakov, A. Y. & Wang, Y. Structure and catalytic performance of alumina-supported copper–cobalt catalysts for carbon monoxide hydrogenation. *J. Catal.* **286,** 51–61 (2012).
7. Palomino, R. M., Magee, J. W., Llorca, J., Senanayake, S. D. & White, M. G. The effect of Fe–Rh alloying on CO hydrogenation to C_{2+} oxygenates. *J. Catal.* **329,** 87–94 (2015).
8. Lopez, L., Velasco, J., Cabrera, S., Boutonnet, M. & Järås, S. Effect of syngas conversion and catalyst reduction temperature in the synthesis of ethanol: concentration of water vapor in mesoporous Rh/MCM-41 catalyst. *Catal. Commun.* **69,** 183–187 (2015).
9. Gupta, M., Smith, M. L. & Spivey, J. J. Heterogeneous catalytic conversion of dry syngas to ethanol and higher alcohols on Cu-Based catalysts. *ACS Catal.* **1,** 641–656 (2011).
10. Spivey, J. J. & Egbebi, A. Heterogeneous catalytic synthesis of ethanol from biomass-derivedsyngas. *Chem. Soc. Rev.* **36,** 1514–1528 (2007).
11. Huang, W. *et al.* Possibility of direct conversion of CH_4 and CO_2 to high-value products. *J. Catal.* **201,** 100–104 (2001).
12. Huang, W., Sun, W. Z. & Li, F. Efficient synthesis of ethanol and acetic acid from methane and carbon dioxide with a continuous, stepwise reactor. *AIChE J.* **56,** 1279–1284 (2010).
13. Belgued, M., Amariglio, A., Paréja, P. & Amariglio, H. Oxygen-Free conversion of methane to higher alkanes through an isothermal two-step reaction on platinum (EUROPT-1): II. hydrogenation of the adspecies resulting from the chemisorption of methane. *J. Catal.* **159,** 449–457 (1996).
14. Amariglio, H., Saint-Just, J. & Amariglio, A. Homologation of methane under non-oxidative conditions. *Fuel Process. Technol.* **42,** 291–323 (1995).
15. Huang, W. Studies on direct of CH_4 and CO_2 to acetic acid by two-step reaction sequen. PhD thesis. *TaiyuanUniversity of Techonology* (2003).
16. Uzunova, E. L., Seriani, N. & Mikosch, H. CO_2 conversion to methanol on Cu(I) oxide nanolayers and clusters: an electronic structure insight into the reaction mechanism. *Phys. Chem. Chem. Phys.* **17,** 11088–11094 (2015).
17. Lee, J. H., Reddy, K. H., Jung, J. S., Yang, E.-H. & Moon, D. J. Role of support on higher alcohol synthesis from syngas. *Appl. Catal. A* **480,** 128–133 (2014).
18. Toniolo, F. S., Magalhães, R. N. S. H., Perez, C. A. C. & Schmal, M. Structural investigation of $LaCoO_3$ and $LaCoCuO_3$ perovskite-type oxides and the effect of Cu on coke deposition in the partial oxidation of methane. *Appl. Catal. B* **117–118,** 156–166 (2012).
19. Fang, Y. Z., Liu, Y. & Zhang, L. H. $LaFeO_3$-supported nano Co-Cu catalysts for higher alcohol synthesis from syngas. *Appl. Catal. A* **397,** 183–191 (2011).
20. Lisi, L. *et al.* Perovskite-type oxides: II. redox properties of $LaMn_{1-x}Cu_xO_3$ and $LaCo_{1-x}Cu_xO_3$ and methane catalytic combustion. *J. Solid State Chem.* **146,** 176–183 (1999).
21. Huang, W., Zuo, Z., Han, P., Li, Z. & Zhao, T. XPS and XRD investigation of Co/Pd/TiO_2 catalysts by different preparation methods. *J. Electron. Spectrosc. Relat. Phenom.* **173,** 88–95 (2009).
22. Angelov, S., Tyuliev, G. & Marinova, T. XPS study of surface composition of polycrystalline $Cu_xCo_{3-x}O_4$ ($0 \leq x < 1$) obtained by thermal decomposition of nitrate mixtures. *Appl. Surf. Sci.* **27,** 381–392 (1987).
23. Fierro, G., Dragone, R., Moretti, G. & Porta, P. XPS investigation on Co-Cu mixed oxide catalysts. *Surf. Inter. Anal.* **19,** 565–571 (1992).
24. Mathew, T., Shiju, N. R., Sreekumar, K., Rao, B. S. & Gopinath, C. S. Cu–Co synergism in $Cu_{1-x}Co_xFe_2O_4$—catalysis and XPS aspects. *J. Catal.* **210,** 405–417 (2002).

25. Zuo, Z. J., Li, J., Han, P. D. & Huang, W. XPS and DFT studies on the autoxidation process of Cu sheet at room temperature. *J Phys Chem C*. **118,** 20332–20345 (2014).
26. Platzman, I., Brener, R., Haick, H. & Tannenbaum, R. Oxidation of polycrystalline copper thin films at ambient conditions. *J Phys Chem C*. **112,** 1101–1108 (2008).
27. Stefanov, P. *et al.* Characterization and catalytic activity of Cu–Co spinel thin films catalysts. *Appl. Surf. Sci.* **245,** 65–72 (2005).
28. Brown, N. M. D., Hewitt, J. A. & Meenan, B. J. X-ray-induced beam damage observed during X-ray photoelectron spectroscopy (XPS) studies of palladium electrode ink materials. *Surf. Inter. Anal.* **18,** 187–198 (1992).
29. Choi, H.-J. & Kang, M. Hydrogen production from methanol/water decomposition in a liquid photosystem using the anatase structure of Cu loaded. *Int. J. Hydrogen Energy* **32,** 3841–3848 (2007).
30. Zhang, S. H. A Study of the Influence of Supports Acidity of the Cu-Co Based catalysts on activation and conversion of methane under mild condition. Master thesis, *Taiyuan University of Technology* (2004).
31. Hao, X., Wang, Q., Li, D., Zhang, R. & Wang, B. The adsorption and dissociation of methane on cobalt surfaces: thermochemistry and reaction barriers. *RSC Adv*. **4,** 43004–43011 (2014).
32. An, W., Zeng, X. C. & Turner, C. H. First-principles study of methane dehydrogenation on a bimetallic Cu/Ni(111) surface. *J. Chem. Phys*. **131,** 174702 (2009).
33. Zhang, W., Wu, P., Li, Z. & Yang, J. First-principles thermodynamics of graphene growth on Cu surfaces. *J Phys Chem C* **115,** 17782–17787 (2011).
34. Shao J., Yuan L., Hu X., Wu Y. & Z. Zhang. The Effect of Nano Confinement on the C–H Activation and its Corresponding Structure-Activity Relationship. *Sci. Rep.* **4,** 7225 (2014)
35. Zuo, Z. J., Huang, W., Han, P. & Li, Z. A density functional theory study of CH_4 dehydrogenation on Co(111). *Appl. Surf. Sci*. **256,** 5929–5934 (2010).
36. Alcalá, R., Mavrikakis, M. & Dumesic, J. A. DFT studies for cleavage of C-C and C-O bonds in surface species derived from ethanol on Pt(111). *J. Catal*. **218,** 178–190 (2003).
37. Liu, H. *et al.* Study on carbon deposition associated with catalytic CH_4 reforming by using density functional theory. *Fuel* **113,** 712–718 (2013).
38. Wang, S. G. *et al.* Kinetic aspect of CO_2 reforming of CH_4 on Ni(111): A density functional theory calculation. *Surf. Sci*. **601,** 1271–1284 (2007).
39. Li, J., Croiset, E. & Ricardez-Sandoval, L. Methane dissociation on Ni (100), Ni (111), and Ni (553): A comparative density functional theory study. *J. Mol. Catal. A* **365,** 103–114 (2012).
40. Choi, Y. & Liu, P. Mechanism of ethanol synthesis from syngas on Rh(111). *J. Am. Chem. Soc*. **131,** 13054–13061 (2009).
41. Zhang, R., Wang, G. & Wang, B. Insights into the mechanism of ethanol formation from syngas on Cu and an expanded prediction of improved Cu-based catalyst. *J. Catal*. **305,** 238–255 (2013).
42. Ayastuy, J. L., Gutiérrez-Ortiz, M. A., González-Marcos, J. A., Aranzabal, A. & González- Velasco, J. R. Kinetics of the low-temperature WGS reaction over a $CuO/ZnO/Al_2O_3$ catalyst. *Ind. Eng. Chem. Res*. **44,** 41–50 (2005).
43. Kowalik, P., Konkol, M., Antoniak, K., Próchniak, W. & Wiercioch, P. The effect of the precursor ageing on properties of the $Cu/ZnO/Al_2O_3$ catalyst for low temperature water–gas shift (LT-WGS). *J. Mol. Catal. A* **392,** 127–133 (2014).
44. Jeong, D. W. *et al.* Hydrogen production from low temperature WGS reaction on co- precipitated $Cu–CeO_2$ catalysts: An optimization of Cu loading. *Int. J. Hydrogen Energy* **39,** 9135–9142 (2014).
45. Zuo, Z. J. Wang, L., Han, P.-D. & Huang, W. Insight into the size effect on methanol decomposition over Cu-based catalysts based on density functional theory. *Comput. Theor. Chem*. **1033,** 14–22 (2014).
46. Mehmood, F., Greeley, J., Zapol, P. & Curtiss, L. A. Comparative density functional study of methanol decomposition on Cu_4 and Co_4 clusters. *J. Phys. Chem. B* **114,** 14458–14466 (2010).
47. Tian, H., Li, X., Zeng, L. & Gong, J. Recent advances on the design of group VIII base-metal catalysts with encapsulated structures. *ACS Catal*. **5,** 4959–4977, (2015).
48. Zeng, B. *et al.* The intrinsic effects of shell thickness on the Fischer-Tropsch synthesis over core-shell structured catalysts. *Catal. Sci. Technol*. **3,** 3250–3255, (2013).
49. Park, J. C. *et al*. Gram-scale synthesis of magnetically separable and recyclable $Co@SiO_2$ yolk-shell nanocatalysts for phenoxycarbonylation reactions. *ChemCatChem* **3,** 755–760 (2011).
50. Liu, P., Logadottir, A. & Nørskov, J. K. Modeling the electro-oxidation of CO and H_2/CO on Pt, Ru, PtRu and Pt_3Sn. *Electrochimica. Acta* **48,** 3731–3742 (2003).
51. Tang, Q. L., Hong, Q. J. & Liu, Z.-P. CO_2 fixation into methanol at Cu/ZrO_2 interface from first principles kinetic Monte Carlo. *J. Catal*. **263,** 114–122 (2009).
52. Cheng, J. & Hu, P. Utilization of the three-dimensional volcano surface to understand the chemistry of multiphase systems in heterogeneous catalysis. *J. Am. Chem. Soc*. **130,** 10868–10869 (2008).
53. Busch, R., Gärtner, F., Borchers, C., Haasen, P. & Bormann, R. High resolution microstructure analysis of the decomposition of $Cu_{90}Co_{10}$ alloys. *Acta Mater*. **44,** 2567–2579 (1996).
54. Bachmaier, A., Pfaff, M., Stolpe, M., Aboulfadl, H. & Motz, C. Phase separation of a supersaturated nanocrystalline Cu–Co alloy and its influence on thermal stability. *Acta Mater*. **96,** 269–283, (2015).
55. Hahn, K. R., Seitsonen, A. P., Iannuzzi, M. & Hutter, J. Functionalization of CeO_2(111) by deposition of small Ni clusters: effects on CO_2adsorption and O vacancy formation. *ChemCatChem* **7,** 625–634 (2015).
56. Chien, C. C., Shi, J. Z. & Huang, T. J. Effect of oxygen vacancy on CO–NO–O_2 reaction over yttria-stabilized zirconia-supported copper oxide catalyst. *Ind. Eng. Chem. Res*. **36,** 1544–1551 (1997).
57. Rodriguez, J. A. *et al.* Gold nanoparticles on ceria: importance of O vacancies in the activation of gold. *Top. Catal*. **44,** 73–81 (2007).
58. Greeley, J. & Mavrikakis, M. Methanol decomposition on Cu(111): A DFT study. *J. Catal*. **208,** 291–300 (2002).
59. Lu, H. *et al.* Selective oxidation of sacrificial ethanol over TiO_2-based photocatalysts during water splitting. *Energ. Environ. Sci*. **4,** 3384–3388 (2011).
60. Yan, J. *et al.* Alcohol induced liquid-phase synthesis of rutile titania nanotubes. *Mater. Sci. Eng. B* **172,** 114–120 (2010).
61. Delley, B. From molecules to solids with the $DMol^3$ approach. *J. Chem. Phys*. **113,** 7756–7764 (2000).
62. Delley, B. An all-electron numerical method for solving the local density functional for polyatomic molecules. *J. Chem. Phys*. **92,** 508–517 (1990).
63. Zuo, Z. J., Wang, L., Han, P.-D. & Huang, W. Insights into the reaction mechanisms of methanol decomposition, methanol oxidation and steam reforming of methanol on Cu(111): A density functional theory study. *Int. J. Hydrogen Energy* **39,** 1664–1679 (2014).
64. Ordejón, P., Artacho, E. & Soler, J. M. Self-consistent order-N density-functional calculations for very large systems. *Phys. Rev. B* **53** R10441–R10444 (1996).
65. Kohn,W. & Sham, L. J. Self-consistent equations including exchange and correlation effects. *Phys. Rev*. **140,** A1133–A1138 (1965).
66. John, P. P. & Wang, Y. Accurate and simple analytic representation of the electron-gas correlation energy. *Phys. Rev. B* **45,** 13244–13249 (1992).
67. Halgren, T. A. & Lipscomb, W. N. The synchronous-transit method for determining reaction pathways and locating molecular transition states. *Chem. Phys. Lett*. **49,** 225–232 (1977).
68. Fehrenbach, G. M. & Bross, H. Self-consistent spline augmented-plane-wave calculation: Ground-state properties of Cu. *Phys. Rev. B* **48,** 17703–17714 (1993).

Acknowledgements

The authors gratefully acknowledge the financial support of this study by the National Basic Research Program of China (2011CB211709), the key project of the National Natural Science Foundation of China (21336006), the National Natural Science Foundation of China (21176167 and 21306125), the key project of Basic Industrial Research of Shanxi (201603D121014), and the Program for the Outstanding Innovative Teams of Higher Learning Institutions of Shanxi.

Author Contributions

Z.-J.Z. studies the ethanol synthesis from CH_4-CO_2 using DFT, the analysis work of XPS, and prepares all the Figures; F.P. studies the experimental work and analysis work except XPS; W.H. plans the experimental work and writes the paper. All authors review the manuscript.

Additional Information

Supplementary information accompanies this paper at http://www.nature.com/srep

Competing financial interests: The authors declare no competing financial interests.

How to cite this article: Zuo, Z.-J. *et al.* Efficient Synthesis of Ethanol from CH_4 and Syngas on a Cu-Co/TiO_2 Catalyst Using a Stepwise Reactor. *Sci. Rep.* **6**, 34670; doi: 10.1038/srep34670 (2016).